

Synthetic Horizons and Thermalization in an Atomic Chain and its Relation to Quantum Hall Systems

Ali G. Moghaddam,^{1,2} Viktor Könye,^{3,4} Lotte Mertens,^{3,4} Jasper van Wezel,⁴ and Jeroen van den Brink^{3,5}

¹*Department of Physics, Institute for Advanced Studies in Basic Sciences (IASBS), Zanjan 45137-66731, Iran*

²*Computational Physics Laboratory, Physics Unit,*

Faculty of Engineering and Natural Sciences, Tampere University, FI-33014 Tampere, Finland

³*Institute for Theoretical Solid State Physics, IFW Dresden and Würzburg-Dresden*

Cluster of Excellence ct.qmat, Helmholtzstr. 20, 01069 Dresden, Germany

⁴*Institute for Theoretical Physics, University of Amsterdam,*

Science Park 904, 1098 XH Amsterdam, The Netherlands

⁵*Institute for Theoretical Physics, TU Dresden, 01069 Dresden, Germany*

(Dated: April 24, 2025)

We investigate the sine model, a one-dimensional tight-binding Hamiltonian featuring hoppings with a sinusoidal dependence on position, and demonstrate the formation of synthetic horizons where electronic wave packets exhibit exponential slowdown. Interestingly, employing the exact transformation between this model and the Harper equation, which describes the eigenstates of a square lattice tight-binding model subjected to perpendicular magnetic field, we find that analogous semi-classical horizons can emerge in a quantum Hall setup at half-filling for specific values of the magnetic flux. Furthermore, by applying sudden quenches to the sine model's hopping profile, we observe the emergence of thermal states characterized by an Unruh temperature. Our numerical calculations of this temperature reveal a non-universal behavior, suggesting the involvement of physical mechanisms beyond a simple low-energy description.

I. INTRODUCTION

One of the fascinating aspects of quantum condensed matter systems lies in the remarkable opportunity to tailor and manipulate them such that they correspond to exotic theoretical models in extreme limits. This allows us to mimic seemingly unrelated physical phenomena within these systems. A prime example is the Sachdev-Ye-Kitaev (SYK) model, initially conceived as a quantum spin system with random, all-to-all interactions, which was later found to have surprisingly profound connections to quantum gravity [1–5]. Another more tangible example is the emergence of Lorentz symmetry in the low-energy description of certain materials, which gives rise to relativistic physics in their continuum limit. Notably, three-dimensional Dirac and Weyl semimetals, as well as two-dimensional graphene, are accurately described by the Dirac equation in their low-energy regimes [6].

Beyond the quantum field theoretic aspects of the above systems, which exhibit features such as the chiral anomaly and the Klein paradox, they offer the exciting possibility of simulating the quantum dynamics of Dirac fermions in curved spacetimes [7–16]. This can be achieved by carefully engineering the material properties to possess an effective position-dependent description [17–19]. Consequently, it becomes feasible to synthesize analogs of general relativistic objects, such as black holes, providing an accessible experimental platform to investigate specific aspects of black hole physics. Numerous setups have been proposed and even implemented to explore this so-called analog gravity within condensed matter systems, including superfluids [20–26], and fermionic or spin systems [27–32], optical and magnonic systems [33, 34], and electronic circuits [35–37].

In this paper, we introduce the sine model, a one-dimensional (1D) tight-binding Hamiltonian characterized by spatially varying hopping amplitudes following a sinusoidal pattern, $\sin(\pi\alpha n)$. This model exhibits horizon physics at the spatial locations where the hopping strength vanishes. In this context, n corresponds to the lattice site index, and the parameter $\alpha = P/N$ takes rational values, where N is the system size and P dictates the number of periods in the sinusoidal modulation. In the low-energy regime, the sine model is equivalent to a 1D chain with a linearly increasing hopping strength [18, 19], which has been shown to allow a direct condensed matter analog for the instantaneous creation of horizons in a gravitational setting [38].

While the sine model holds significant intrinsic interest, as evidenced by its potential realization in experimental platforms such as ultracold atoms in optical lattices with modulated inter-site coupling and in metamaterials, it also exhibits a profound relationship with the integer quantum Hall effect in a square lattice through its description in terms of the Harper's equation. Indeed, a specific gauge transformation establishes a mapping between the Harper model [39, 40] and the sine model, and vice versa. In the context of the quantum Hall effect, the magnetic flux Φ per unit cell, when expressed in units of the flux quantum Φ_0 as $\alpha = \Phi/\Phi_0$, determines the key parameter α . In typical scenarios, this corresponds to a regime of weak magnetic field and large magnetic length. Furthermore, at the electron-hole symmetric point of half-filling, this setup leads to the closure of the energy gap and the emergence of zero-energy modes [41], resulting in a non-quantized Hall conductance [42]. In direct correspondence with the sine model, we also demonstrate the formation of semi-classical hori-

zons in the Harper model, where electron wave packets exhibit exponential slowing down on the separatrices of its phase portrait. Numerical simulations of wave packet propagation in the quantum model corroborate these analytical findings and their limitations.

Furthermore, we demonstrate the emergence of (almost) thermal states and an associated Unruh temperature through sudden quenches in the hopping profile of the sine model. Specifically, starting from the quantum ground state of the sine model at zero temperature for a given P , and by abruptly increasing the number of periods, or equivalently the number of horizons, across the chain by an integer ΔP , we observe this thermalization. This process, driven by the formation of new horizons, leads to an Unruh temperature given by $k_B T/E_F = c\Delta P$, which originates from the entanglement present in the pre-quench multi-particle ground state across the newly formed horizon. Our direct numerical calculations yield the Unruh temperature and the constant of proportionality c , revealing a non-universal behavior. This non-universality indicates that the flux quench in the sine model involves processes that extend beyond the description provided by the effective low-energy Hamiltonian of a chain with linearly increasing hopping.

II. HORIZON PHYSICS IN THE HARPER AND SINE MODELS

A. Sine model

We begin by introducing the *sine hopping model*, which is defined on a 1D lattice with sites $n \in [0, N-1]$ and described by the Hamiltonian

$$\hat{H}_S = \sum_{n=0}^{N-2} 2 \sin(\pi\alpha n) \hat{c}_n^\dagger \hat{c}_{n+1} + h.c., \quad (1)$$

where \hat{c}_n^\dagger and \hat{c}_n are the fermionic creation and annihilation operators at site n , respectively. The parameter α is a rational number, which can be expressed as $\alpha = P/N$, where P is the number of periods in the sine modulation and N is the system size. The Hamiltonian (1) describes a tight-binding model with nearest-neighbor hopping, where the hopping amplitude varies sinusoidally with the lattice site index n . The eigenvalue equation for the sine model is thus given by set of coupled equations

$$2 \sin(\pi\alpha n) \phi_{n-1} + 2 \sin(\pi\alpha(n+1)) \phi_{n+1} = \epsilon \phi_n, \quad (2)$$

for the eigenvalue ϵ .

In the vicinity of points where the hopping amplitude vanishes, the sine model exhibits a synthetic horizon similar to that in linearly increasing hopping models [18, 19, 38]. To see this, it is helpful to first consider the sine model in the continuum limit (see Appendix A), where the Hamiltonian can be expressed as

$$\hat{\mathcal{H}}_S = 4 \cos(\hat{p}) \sin(\pi\alpha\hat{x}). \quad (3)$$

Hence, the hopping amplitude vanishes at points

$$x_h \equiv \frac{m}{\alpha}, \quad (4)$$

where $m \in \mathbb{Z}$, and x_h is a continuous parameter that coincides with n_h at integer values. In the vicinity of such points, the sine model can be approximated by a tight-binding chain with linearly increasing hopping strengths:

$$\epsilon \phi_n = \pi\alpha [n\phi_{n-1} + (n+1)\phi_{n+1}], \quad (5)$$

which harbors the synthetic horizons.

B. Harper's model

Next, we consider the Landau-gauge Schrödinger equation for 2D lattice electrons in a magnetic field which reduces, after a Fourier transform of one of the spatial directions, to the well-known 1D Harper's equation [39, 40, 43–45]

$$\psi_{j-1} + 2 \cos(2\pi\alpha j + \theta) \psi_j + \psi_{j+1} = \epsilon \psi_j. \quad (6)$$

Here, the wave function ψ_j is defined on discrete lattice sites $j \in [0, N-1]$, the energy is denoted by ϵ , and $\theta \in \mathbb{R}$ is the quasi-momentum corresponding to the Fourier transformed spatial direction. Finally, α is equal to the magnetic flux through a lattice cell divided by the magnetic flux quantum. Note that the energy ϵ is measured in units of the hopping amplitude λ , so that a half-filled band with particle-hole symmetry has Fermi energy $E_F = 2\lambda$.

The continuum form of the Harper equation is given by

$$\hat{\mathcal{H}}_H = 2 \cos(\hat{q}) + 2 \cos(2\pi\alpha\hat{y} + \theta), \quad (7)$$

where \hat{q} and \hat{y} denote the momentum and position operators, respectively (see Appendix A). As mentioned in the introduction and detailed later, an exact mapping exists between the sine model and the Harper equation. In the continuum limit, this mapping can be readily established through the following canonical transformation:

$$\hat{q} = -\hat{p} + \pi\hat{x}\alpha - \frac{\pi}{2}, \quad (8)$$

$$2\pi\alpha\hat{y} = \hat{p} + \pi\hat{x}\alpha - \theta - \frac{\pi}{2}. \quad (9)$$

The connection between these two models can be elegantly visualized through the phase portraits of their respective continuum Hamiltonians in the classical limit. The phase portraits for the Harper and sine models are depicted in Fig. 1, each comprising two lattices of closed orbits separated by separatrix lines (dashed in black). Consistent with the canonical transformation provided above, the two phase portraits are related by a combination of shift, rescaling, and rotation.

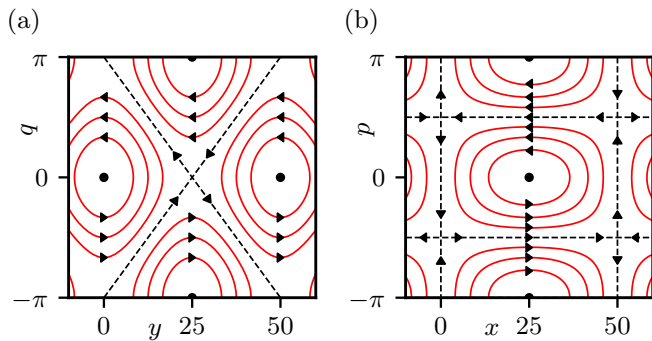


FIG. 1. Phase-portraits for Harper's equation (a) and the sine model (b), with $\alpha = 1/50$ and $\theta = 0$. The center for the circular solutions is given by the black dot at $q = 0$ and $p = 0$. The portraits are related by a rotation of $\pi/4$ and a shift of the centers, as well as a rescaling. The black dashed lines indicate the separatrices.

Importantly, the canonical transformation between the continuum-limit Hamiltonians preserves the classical trajectories, which exhibit an exponential slowdown characteristic of horizon physics in both the sine and Harper models. Restricting to a separatrix, the Heisenberg equations of motion yield the following time dependence for the classical expectation value of position (as detailed in Appendix A):

$$y(t) = \frac{1}{\pi\alpha} \left[\arctan \left(e^{-4\pi\alpha(t-t_0)} \right) - \theta/2 \right] + \frac{1}{2\alpha}. \quad (10)$$

As anticipated for a separatrix in a classical phase portrait, the position exponentially slows down as it approaches the intersection with another separatrix. It is pertinent to consider the quantum analog at this juncture. While the centers of time-evolving wave packets in the Harper equation will initially follow the classical trajectories on the separatrix, it becomes evident that in the quantum regime, the wave packet cannot continuously slow down and localize indefinitely. Eventually, when the wave packet's width becomes comparable to the lattice spacing, the semi-classical description breaks down. Indeed, the unitary evolution of quantum mechanical wave packets leads to their disintegration at the horizon due to the presence of a high-energy cutoff on the lattice [18].

C. Exact map Between the Harper and sine models

As previously mentioned, an exact mapping exists between the Harper equation and the sine model [39, 40]. This mapping holds for the discrete lattice versions of both models (i.e., beyond the continuum limit) under the following conditions, detailed in Appendix B:

1. P and N are coprime.
2. $\theta = (2m' + 1)\frac{\pi}{N}$ with $m' \in \mathbb{Z}$.

This mapping is crucial for connecting the numerical simulations of wave packet dynamics in the Harper model to the horizon physics observed in that model, and similarly for the sine model. Subject to the conditions above, an eigenfunction ϕ_m of the sine model is mapped to an eigenfunction ψ_n of the Harper equation by:

$$\psi_n = \frac{1}{N} \sum_k^{N-1} e^{ik(\theta-\pi)} e^{i\pi\alpha[2nk+(k+\frac{1}{2})^2]} \sum_m^{N-1} i^{-m} e^{i\pi\alpha[2km+\frac{m(m+1)}{2}]} \phi_m. \quad (11)$$

III. WAVE PACKET DYNAMICS NEAR THE HORIZON

It has been established previously [18, 19, 38, 46, 47] that models with position-dependent nearest-neighbor hopping can have dynamics of zero-energy wave packets that coincide with the dynamics of Dirac fields in a static curved spacetime. The semi-classical mapping also manifests in the dynamics of coherent wave packets in the current model, which we will explore by numerical simulation. For Harper's model the horizon encountered on the separatrices is located at $y_h \equiv \frac{2m+1}{2\alpha} - \frac{\theta}{2\pi\alpha}$ for $m \in \mathbb{Z}$, corresponding to the crossing point of the dashed black lines in the semi-classical phase portrait of Fig. 1(a). For a coherent wave packet around a given initial momentum and position, the phase portrait for the evolution of its center of mass is shown in Fig. 2. This figure shows that the quantum evolution of the wave packet's centre of mass matches the previous semi-classical analysis. At initial momenta close to $q = 0$, harmonic oscillations are recovered, while for momenta on the separatrices, the evolution asymptotically approaches the horizon at $q = 0$ and $y = y_h$ while exponentially slowing down, until the wave packets become delocalized as finite size effects take over.

For both Harper's equation and the sine model, a set of synthetic horizons arise, as witnessed by wave packets exponentially slowing down and never reaching x_h or y_h (for a detailed calculation, see Appendix A).

The main difference between the two models is visible when we consider the evolution of q as the wave packet approaches the horizon. For the sine model, starting from $p = \pi/2$, the momentum stays constant over the whole trajectory. But for Harper's equation, $d\hat{q}/dt$ only becomes zero at the horizon: it changes along the trajectory. This is due to the canonical transformations which render horizontal lines in the phase portrait of one model diagonal in that of the other.

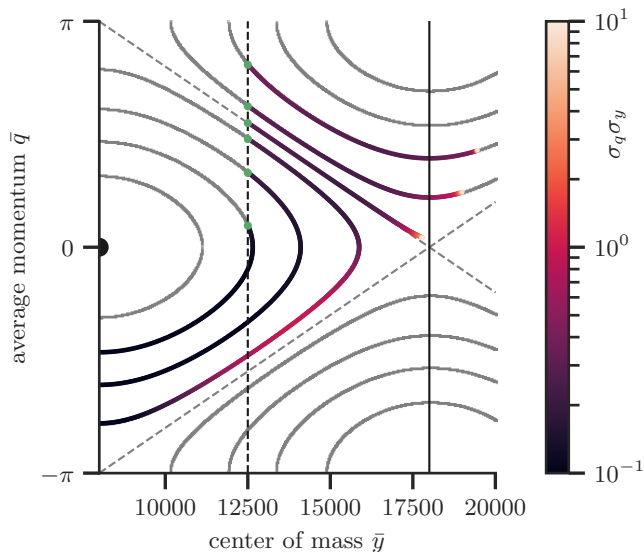


FIG. 2. Time evolution of wave packets in Harper's model, Eq. (6), where the initial wave packet has a momentum between $-\pi$ and π . All wave packets start at the dashed black line at lattice point 12500. The color of the lines denotes $\sigma_q \sigma_y$, the product of the instantaneous standard deviations in momentum and position of the wave packet. When this becomes large, the wave packet is no longer localized, and the simulation is stopped. The vertical black line marks the position of the horizon encountered along the separatrix, which lies at $y_h = 18000$ with $P = 1$ and $N = 20008$, while the gray lines mark semiclassical trajectories.

IV. THERMALIZATION IN THE SINE MODEL

We have shown the correspondence between the sine model and Harper's equation in terms of their synthetic horizons, both semiclassically and for wave packet dynamics. This sets us up to consider the emergence of thermal radiation in the quantum state of free fermions upon a sudden change in the periodicity of the sine model, in analogy to the thermal behavior previously observed after a quench in the linear hopping model [38].

Thermalization in gravity is well-known in the context of Hawking and Unruh radiations, where the presence of a horizon makes part of the ground state unobservable to observers on each side of the horizon [48, 49]. This causes the quantum vacuum to appear as a mixed thermal state for those observers [50–54]. As an alternative route to understanding the emergence of thermal quantum states in the presence of a horizon, we will study the thermalization in the sine model and show that it mimics the thermal behavior found in the gravitational setting.

To calculate the thermalization, we consider an instantaneous increase in the number of periods P that creates one or more synthetic horizons in the lattice model with sinusoidal hopping. The effect of this change is characterized by calculating the number of excitations present in the system before and after the horizon's formation, in terms of instantaneous eigenstates of the Hamiltonian.

Such a boost results in an emergent temperature in the sine model equal to the analog Unruh temperature. This has been previously shown for an N -site chain with homogeneous hopping quenched to one with linearly increasing hopping, which gives rise to the Unruh temperature $T = \frac{2\lambda}{N\pi}$ for large N (considering $k_B = 1$), with λ indicating the slope of the linear dependence of the hopping parameter [38]. The underlying reason for the excited state distribution to be precisely thermal was shown in that case to be that the post-quench Hamiltonian matches the entanglement Hamiltonian of the pre-quench system. The connection between the post-quench Hamiltonian and entanglement Hamiltonian corresponding to the ground state of the pre-quench system also applies to the sine model in at least one type of quench: it has been shown that the half-system entanglement Hamiltonian of a finite ring of size L and under periodic boundary conditions approaches a position-dependent Hamiltonian density $\sin(2\pi x/L)\mathcal{H}$ where \mathcal{H} denotes the original system Hamiltonian density [55–58]. These works, which are based on $(1+1)D$ conformal field theory and numerical evaluations of tight-binding chains, provide extensions of the Bisognano-Wichmann theorem relating the entanglement Hamiltonian of a generic relativistic quantum field to the boost operator [59–61].

Considering a particular quench from a uniform hopping model at half-filling and under periodic boundary conditions to a sine model with $P = 2$ with a pair of horizons, an exactly thermal distribution is obtained whose Unruh temperature is $T = 2\lambda/N = E_F \Phi/\Phi_0$. This has been illustrated in Fig. 3(a) where the post-quench excitation spectrum is shown for different lengths. In this case, there is an exact mapping to the entanglement Hamiltonian as mentioned earlier, which results in an exact Fermi-Dirac (FD) distribution for the expectation value of the post-quench modes' occupation number $\langle b_E^\dagger b_E \rangle$. Here, b_E^\dagger and b_E correspond to the creation and annihilation operators of a post-quench eigenstate with energy E (for details on how this is calculated see Appendix C).

We note that the lattice sizes used in Fig. 3 are chosen to be multiples of two but not four, such that each causally connected post-quench region contains an odd number of sites, ensuring the existence of a post-quench zero-energy mode. As discussed in detail in Appendix C, for lattice sizes that are multiples of four, the thermal behavior is less accurately reproduced for finite sizes, but it asymptotically approaches the thermal form as the lattice length increases. This type of even-odd effect, which depends on the number of sites (and thus states) within each post-quench sub-region, is a generic feature that persists even for large but finite system sizes.

Going beyond the quench from flat space to $P = 1$, we also numerically examine the thermalization following a sudden quench from $P = 1$ to $P = 2$ as shown in Fig. 3(b). The resulting distribution in this case is approximately thermal, as indicated by slight deviations from the Fermi-Dirac distribution. These devia-

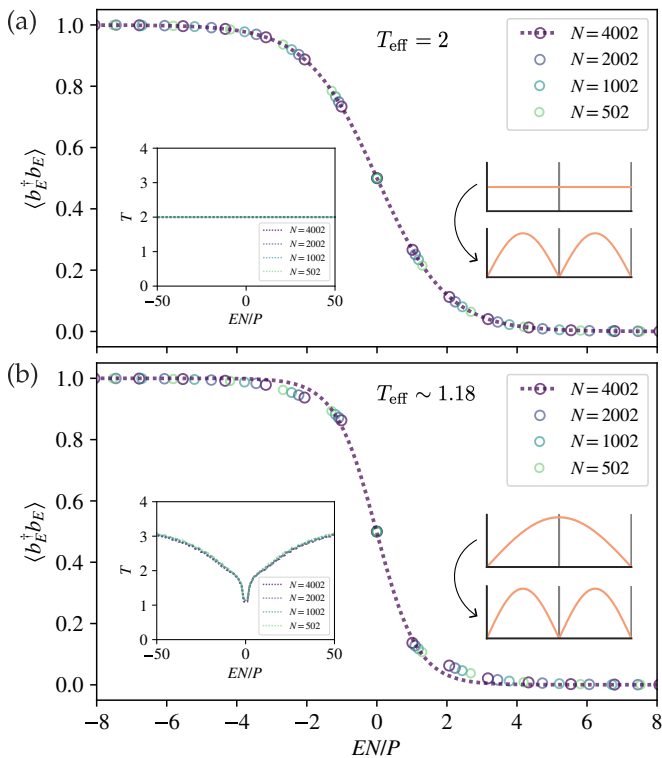


FIG. 3. Expectation values of the occupation number $\langle b_E^\dagger b_E \rangle$ for post-quench modes, together with corresponding fits using a thermal FD distribution. Panel (a) corresponds to a quench from the constant hopping model to the sinusoidal hopping model with $P = 2$. Panel (b) shows a similar plot but for a quench between sinusoidal hopping models from $P = 1$ to $P = 2$. The insets show the variation of the energy-dependent effective temperature $T(E)$, assuming a generalized thermal form $[1 + \exp(E/T(E))]^{-1}$. While panel (a) displays an exact thermal form, panel (b) exhibits deviations from the exact FD form, evidenced by the non-constant effective temperature $T(E)$ in the inset of (b).

tions are also evident in the energy-dependent temperature $T(E)$, derived by applying the inverse Fermi-Dirac function to the numerically obtained distribution. The effective temperature obtained from fitting is approximately half of that observed in Fig. 3(a). The deviation from pure thermalization is expected because the entanglement Hamiltonian of the pre-quench state, characterized by a sine profile, no longer perfectly matches the post-quench Hamiltonian. Nevertheless, the Fermi-Dirac function remains a very good approximation, with a very small fitting error of $\chi \sim 0.05 \ll 1$ for $N = 4002$, which decreases with increasing N [62]. Additionally, we note that while the energy-dependent temperature $T(E)$ varies significantly between low- and high-energy states, the average temperature obtained from fitting is primarily determined by the low-energy states, which are more sensitive to the thermalization.

In the following, we consider a larger boost, for example, increasing from $P = 1$ to $P = 3$, under which the post-quench system develops multiple horizons and

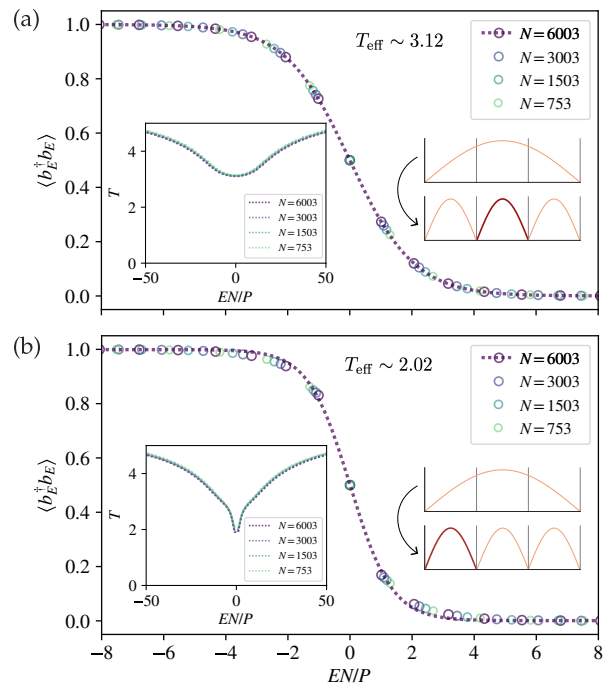


FIG. 4. Expectation values of the occupation number $\langle b_\omega^\dagger b_\omega \rangle$ for post-quench modes are shown, similar to the results in Fig. 3, but for a quench between sinusoidal hopping models from $P = 1$ to $P = 3$. Panels (a) and (b) display the results for the average mode occupations in the middle and side regions, respectively, as illustrated in the two schematic insets. We observe that the middle region has a higher effective temperature, and its distribution is closer to a FD form compared to that of the side regions.

distinct causally disconnected subregions. By analyzing the mode occupation and effective temperature within each region bounded by adjacent horizons, we find that each subregion acquires its own characteristic temperature. Additionally, we show that deviations from a perfectly thermal distribution also manifest as small but non-vanishing off-diagonal correlations, $\langle b_{E'}^\dagger b_E \rangle$, near $E, E' \approx 0$.

A. Regions with different temperatures

An interesting situation arises by considering, for instance, boost from $P = 1$ to $P = 3$ where the pre-quench model contains qualitatively different regions, as shown in Fig. 4(a). As the post-quench model contains multiple horizons, we separately consider the distribution of the mode occupations between each pair of neighboring horizons. Each of the disconnected post-quench regions is characterized by an individual temperature. In the pre-quench model, the three post-quench regions marked in Fig. 4(a) are inequivalent. The middle region spans the approximately flat part of the $P = 1$ sinusoidal hopping profile, while the outer regions contain approximately linear parts. The temperature in the middle region is found

to be higher than on the two outside regions as anticipated by comparison to the previous results shown in Fig. 3. In both cases the temperature is larger when the pre-quench Hamiltonian over the region of interest is (almost) flat compared to the case where pre-quench Hamiltonian has (almost) linear profile.

We also see that the distributions for both middle and side regions in this case are not exactly thermal as reflected in the energy dependence of $T(E)$ shown in the insets of Fig. 4. However, the distribution for the middle region is much more closer to an exact Fermi-Dirac distribution, with a fitting error of $\chi \sim 10^{-3}$ compared to the side regions, for which the error is $\chi \sim 10^{-2}$. Similarly, for the more generic case of quenching from P_1 to P_2 we expect thermalization to be closer to ideal in the regions where the pre-quench profile is almost flat. In that case the temperature is mainly determined by the post-quench profile, and approximately scales as $T \propto P_2$ due to the increase in surface gravity by quenching to P_2 .

B. Off-diagonal correlations

In this section, we examine how the slight deviations from an exact thermal distribution are reflected in the off-diagonal correlations between different energies, denoted as $\langle b_E^\dagger b_{E'} \rangle$.

As shown in Fig. 5(a), when the expectation values for the occupation numbers of post-quench modes are exactly thermal, there are no off-diagonal correlations between different energy modes. Conversely, slight deviations from the exact thermal distribution, such as those occurring when quenching from the sine models with $P = 1$ to $P = 2$, are accompanied by deviations from a purely diagonal form. This is illustrated in Fig. 5(b), where small nonzero off-diagonal correlations appear near the zero modes, $E, E' \sim 0$.

As we move away from the zero modes to a region in which the diagonal terms corresponding to the expectation values of the occupation numbers closely approach zero or one, the off-diagonal terms are suppressed, as expected. Similar behavior, characterized by simultaneous deviations from the thermal form of the diagonal terms and small non-zero off-diagonal terms around zero energy, is observed in other cases, such as quenching from $P = 1$ to $P = 3$, and other such quenches.

V. DISCUSSION AND SUMMARY

We used a direct connection between quantum Hall states in a lattice described by Harper's model and a 1D sinusoidal hopping model to explore analog gravitational features in both. We first showed the correspondence between the two models by studying semiclassical equations of motions and wave-packet dynamics on a lattice. It has been found that both Harper's model and the sine model host synthetic horizons, where quasiparticles slow down

exponentially and localize until finite-size effects lead to their disintegration.

Our findings regarding the quantum Hall system suggest a direct generalization: synthetic horizons and thermalisation may be expected to arise in *any* quantum lattice system where a saddle point in the semi-classical continuum phase portrait causes classical particles to slow down exponentially. Similar to the findings presented here, the dynamics of coherent wave packets under the full quantum evolution may then be expected to follow the semiclassical path, until a point where the finite lattice spacing forces the wave packets to disintegrate.

Furthermore, we demonstrated the potential of the *sine model* to act as a fundamental tool for studying Unruh-like effects and thermalization resulting from sudden changes in the periodicity of the sinusoidal hopping profile. That the post-quench mode occupation is precisely thermal is not a universal occurrence; it manifests only when the so-called entanglement Hamiltonian of the pre-quench system closely approximates the actual Hamiltonian of the post-quench system [38]. The entanglement Hamiltonian in the sine model *equals* the post-quench Hamiltonian for a quench from uniform to a single sine hopping profile ($P = 0$ to $P = 1$), and we confirmed the resulting purely thermal occupation profile.

It might seem intuitive that the exact mapping between the sine and Harper models would allow for the engineering of similar thermalization phenomena in a quantum Hall system by simply and suddenly changing the magnetic flux. However, this direct approach does not give rise to thermalization. While all other results presented in this work rely on the exact mapping between sine model and Harper's equation for a single integer P , the situation becomes more complex when considering quench-induced thermalization due to the creation of new horizons. This is because such scenarios involve two Hamiltonians (in either the sine or Harper's model description, corresponding to pre- and post-quench Hamiltonians) with different values of P . Given that the precise form of the transformation depends on the value of P , applying the transformation corresponding to the post-quench Hamiltonian from the sine to the Harper model, for instance, necessitates applying the same transformation to the ground state corresponding to the pre-quench Hamiltonian (which has a different P). This leads to a highly intricate and contrived initial state, very different from the typical ground states of a simple Harper or sine model. Therefore, observing any quench-induced Unruh temperatures in the quantum Hall setting would require careful engineering of the initial state.

Both the sine and Harper models can be readily realized and controlled in cold atom setups [63, 64]. The formation of horizons and the exponential slowdown of wave packets can also be observed in these systems by dynamically generating wave packet-like excitations and allowing them to evolve. Furthermore, the Unruh effect predicted for the sine model upon performing sudden quenches, as a fully quantum phenomenon that depends

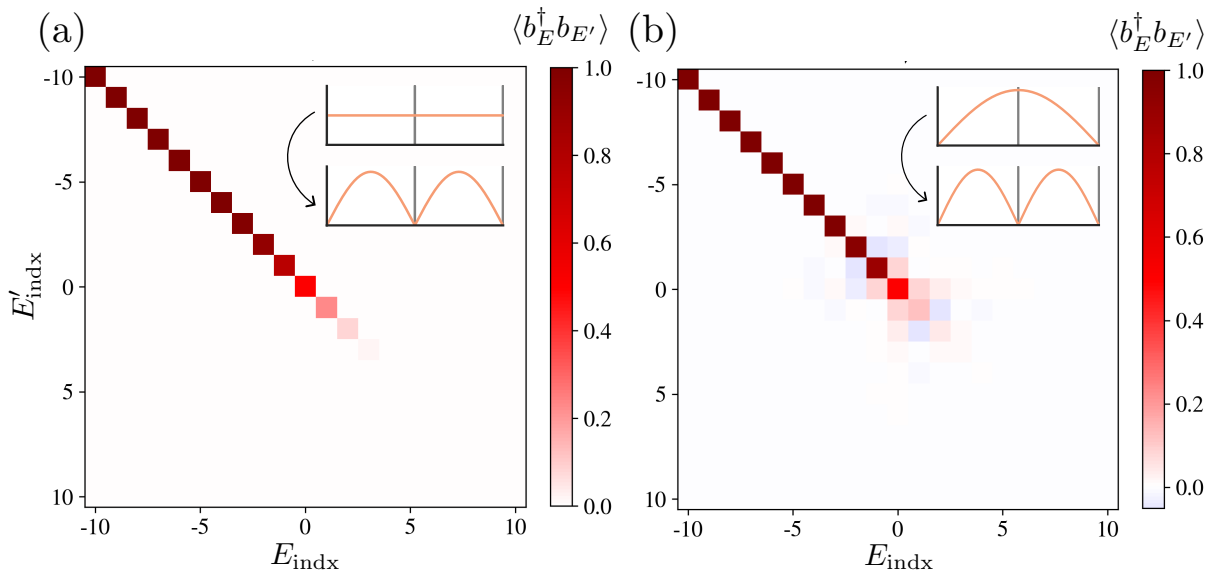


FIG. 5. Correlation matrix elements for post-quench modes, $\langle b_E^\dagger b_{E'} \rangle$. The comparison is made between (a) a quench from $P = 0$ to $P = 2$, and (b) a quench from $P = 1$ to $P = 2$, as illustrated in the insets. In panel (a), we observe a perfect thermal distribution with no off-diagonal correlations. In contrast, panel (b) shows some nonzero off-diagonal correlations around zero energy, along with deviations from the perfect thermal form for the diagonal elements, as discussed in the main text. The results are obtained for a lattice size of $N = 1002$. Note that E_{indx} and E'_{indx} represent the indices of the eigenvalues of the post-quench Hamiltonian for a sub-region, with $E_{\text{indx}} = 0$ corresponding to the zero-energy state.

on the multi-particle fermionic nature of the model, can also be explored in cold atom experiments. Moreover, since the wave packet dynamics is fundamentally a single-particle phenomenon, it does not depend on the fermionic statistics of the underlying system and can therefore also be studied in photonic metamaterials or electrical circuits that effectively model the sinusoidal hopping of the sine model or the potential modulation in the case of the Harper model.

The sine model and its connection with Harper's equation thus provide a convenient platform for exploring horizon physics and thermalisation in analog gravity, in which particle dynamics as well as the causes, consequences, and non-universal features of thermalisation can be studied.

Acknowledgments

This work was supported by the Deutsche Forschungsgemeinschaft (DFG, German Research Foundation) through the Sonderforschungsbereich SFB 1143, grant No. YE 232/2-1, and under Germany's Excellence Strategy through the Würzburg-Dresden Cluster of Excellence on Complexity and Topology in Quantum Matter – *ct.qmat* (EXC 2147, project-ids 390858490 and 392019). A.G.M. acknowledge Jane and Aatos Erkkö Foundation for financial support.

Appendix A: Continuum models

1. Harper's model

We start by considering Harper's equation [43]:

$$\psi_{n-1} + 2 \cos(2\pi\alpha n + \theta)\psi_n + \psi_{n+1} = \epsilon\psi_n. \quad (\text{A1})$$

where the state ψ_n is defined on discrete lattice sites $n \in [0, N - 1]$, the energy is denoted by ϵ , and $\theta \in \mathbb{R}$ is the quasi-momentum corresponding to the Fourier transformed spatial direction. Finally, $\alpha = P/N$ is equal to the magnetic flux through a lattice cell divided by the magnetic flux quantum.

By going to very large systems $N \rightarrow \infty$ and $\alpha \rightarrow 0$ we can construct the semiclassical limit of the Harper's equation. The ψ_n eigenstate is replaced by $\psi(y)$ with $\psi(n) = \psi_n$. For large enough N we can think of $\psi(y)$ as a continuous differentiable function.

The Harper's equation in this approximation becomes

$$\psi(y+1) + \psi(y-1) + 2 \cos(2\pi\alpha y + \theta)\psi(y) = \epsilon\psi(y). \quad (\text{A2})$$

We introduce the position operator \hat{y} and the conjugate momentum \hat{q} with commutation relation $[\hat{y}, \hat{q}] = i$. Translations are generated by \hat{q} and the shifted wave function can be expressed as

$$\psi(y+1) = e^{i\hat{q}}\psi(y). \quad (\text{A3})$$

With this, the Harper's equation can be expressed as

$$\hat{\mathcal{H}}_H\psi(y) = \epsilon\psi(y), \quad (\text{A4})$$

with the corresponding Hamiltonian

$$\hat{\mathcal{H}}_H = 2 \cos(\hat{q}) + 2 \cos(2\pi\alpha\hat{y} + \theta). \quad (\text{A5})$$

For this Hamiltonian, we can calculate the semiclassical dynamics. The Heisenberg equations of motion yield

$$\begin{aligned} \frac{d\hat{y}}{dt} &= i[\hat{\mathcal{H}}_H, \hat{y}] = -2 \sin(\hat{q}), \\ \frac{d\hat{q}}{dt} &= i[\hat{\mathcal{H}}_H, \hat{q}] = 4\pi\alpha \sin(2\pi\alpha\hat{y} + \theta). \end{aligned}$$

Using these equations and the Ehrenfest theorem we can get the semiclassical dynamics of $y = \langle \hat{y} \rangle$ and $q = \langle \hat{q} \rangle$ by replacing the operators with their expectation value in the Heisenberg equations of motion. We can solve these equations using

$$\frac{dq}{dy} = -2\pi\alpha \frac{\sin(2\pi\alpha y + \theta)}{\sin(q)}, \quad (\text{A6})$$

which has linear solutions (this will lead to solutions on the separatrices)

$$q = 2\pi\alpha y + \theta + (2m + 1)\pi, \quad (\text{A7})$$

where $m \in \mathbb{Z}$. With this, the time evolution of the position $y(t)$ becomes

$$y(t) = \frac{1}{\pi\alpha} \arctan\left(e^{-4\pi\alpha(t-t_0)}\right) - \frac{\theta}{2\pi\alpha} - \frac{2m+1}{2\alpha}. \quad (\text{A8})$$

This solution shows exponential slowing down for $t \rightarrow \infty$, at $y = -\theta/(2\pi\alpha) - \frac{2m+1}{2\alpha}$. Similarly, the time dependence for q becomes

$$q(t) = 2 \arctan\left(e^{-4\pi\alpha(t-t_0)}\right) + 2n\pi,$$

where $n \in \mathbb{Z}$. At $t \rightarrow \infty$ this reduces to $2n\pi$. Away from the separatrix, different solutions exist, as shown in Fig. 1 in the main text.

For example, at $q = q'$ and $y = -\theta/(2\pi\alpha) + y'$ for small q', y' the Hamiltonian becomes

$$\hat{\mathcal{H}}_H \approx 4 + (q')^2 + (2\pi\alpha y')^2.$$

This is the formula for a quantum harmonic oscillator which give the circular orbits in Fig. 1 of the main text.

2. Sine model

The sine model is defined as

$$2 \sin(\pi n\alpha)\phi_{n-1} + 2 \sin(\pi(n+1)\alpha)\phi_{n+1} = \epsilon\phi_n, \quad (\text{A9})$$

In the semiclassical limit, similarly to the previous section (now position and the conjugate momentum are \hat{x} and \hat{p}) for the Hamiltonian we get [65]

$$\hat{\mathcal{H}}_S = 2 \sin(\pi\hat{x}\alpha)e^{-i\hat{p}} + 2 \sin(\pi(\hat{x}+1)\alpha)e^{i\hat{p}}. \quad (\text{A10})$$

For large enough systems where $\alpha \rightarrow 0$ we can approximate the Hamiltonian as

$$\hat{\mathcal{H}}_S \approx 4 \sin(\pi\hat{x}\alpha) \cos(\hat{p}). \quad (\text{A11})$$

Using the Heisenberg equations of motion for the sine model we get

$$\frac{d\hat{x}}{dt} = i[\hat{\mathcal{H}}_S, \hat{x}] = -4 \sin(\pi\hat{x}\alpha) \sin(\hat{p}), \quad (\text{A12})$$

$$\frac{d\hat{p}}{dt} = i[\hat{\mathcal{H}}_S, \hat{p}] = -4\alpha\pi \cos(\pi\hat{x}\alpha) \cos(\hat{p}). \quad (\text{A13})$$

This coincides with the result known for a model with linearly increasing hopping strength [38], in which a wave packet centered at $p \equiv \langle \hat{p} \rangle = \pm\pi/2$ has constant momentum and a trajectory given by

$$x(t) = \frac{2}{\pi\alpha} \arctan\left(e^{\mp 4\pi\alpha(t-t_0)}\right) + \frac{2m}{\alpha}, \quad (\text{A14})$$

where $m \in \mathbb{Z}$. For $t \rightarrow \infty$ there are multiple horizons at $x_h = x(t = \infty) = m'/\alpha$ for $m' \in \mathbb{Z}$.

We can write an effective continuum model for momenta close to $p = \pm\pi/2$ and near the horizons. Taking $\alpha = 1/N$ we have the horizons at $x = 0$ and $x = N$. Close to the left and right horizon we introduce small parameters x' and p'

$$\hat{x} = \hat{x}' \quad \hat{p} = \pi/2 + \hat{p}', \quad (\text{A15})$$

$$\hat{x} = N + \hat{x}'' \quad \hat{p} = -\pi/2 + \hat{p}''. \quad (\text{A16})$$

Substituting to Eq. (A10) the effective Hamiltonian becomes

$$\hat{\mathcal{H}}'_S \approx -2\pi\alpha(\hat{x}'\hat{p}' + \hat{p}'\hat{x}'), \quad (\text{A17})$$

$$\hat{\mathcal{H}}''_S \approx 2\pi\alpha(\hat{x}''\hat{p}'' + \hat{p}''\hat{x}''). \quad (\text{A18})$$

This is proportional to the Keating-Berry operator.

Appendix B: Transformation from Harper's equation to the sine model

Following the transformations introduced in Ref. [40], we will show how the Harper's model can be transformed to the sine model. We can re-write Harper's Eq. (6) as

$$\psi_{n-1} + (q^{2n}e^{i\theta} + q^{-2n}e^{-i\theta})\psi_n + \psi_{n+1} = \epsilon\psi_n, \quad (\text{B1})$$

where $q \equiv e^{i\pi\alpha}$. We consider periodic boundary conditions given by $\psi_N = \psi_0$. We define the following transformation

$$\psi_n = \frac{1}{\sqrt{N}} \sum_{k=0}^{N-1} q^{2nk} e^{ik(\theta-\theta')} \chi_k, \quad (\text{B2})$$

with inverse transformation

$$\chi_k = \frac{1}{\sqrt{N}} \sum_{n=0}^{N-1} q^{-2nk} e^{-ik(\theta-\theta')} \psi_n, \quad (\text{B3})$$

where $\theta' \in \mathbb{R}$ is introduced as a free parameter (its function will become evident later). We note that the inverse transformation (B3) implies a periodicity condition

$$\chi_{k+N} = e^{-iN(\theta-\theta')} \chi_k, \quad (\text{B4})$$

and in particular $\chi_N = e^{-iN(\theta-\theta')} \chi_0$. The inverse transformation is consistent only when N and P are co-primes in $\alpha = P/N$. The reason is that we require the so-called completeness condition

$$\sum_{k=0}^{N-1} q^{2nk} = N\delta_{n,0}, \quad (\text{B5})$$

which in turn is valid only when there is no other integer than $n = 0$ in the range of $[0, N-1]$ for which $q^{2n} = 1$. If P and N have a common divisor larger than 1 then, there will be other n 's for which $q^{2n} = 1$ and the completeness is not satisfied.

Inserting Eq. (B2) into Eq. (B1) yields

$$\begin{aligned} & \sum_{k=0}^{N-1} \left[q^{2(n-1)k} e^{ik(\theta-\theta')} + q^{2n(k+1)} e^{ik(\theta-\theta')+i\theta} \right. \\ & \left. + q^{2n(k-1)} e^{ik(\theta-\theta')-i\theta} + q^{2(n+1)k} e^{ik(\theta-\theta')} \right] \chi_k \\ & = \epsilon \sum_{k=0}^{N-1} q^{2nk} e^{ik(\theta-\theta')} \chi_k. \end{aligned}$$

The middle two terms can be rewritten by defining $k' = k \pm 1$. This gives a sum that is shifted by ± 1 from the desired domain. This leaves us with the equation

$$e^{i\theta'} \chi_{k-1} + (q^{2k} + q^{-2k}) \chi_k + e^{-i\theta'} \chi_{k+1} = \epsilon \chi_k. \quad (\text{B6})$$

We apply a second transformation, given by

$$\chi_k = \frac{1}{\sqrt{N}} \sum_{n=0}^{N-1} q^{(k+1/2)^2} q^{2kn} \zeta_n. \quad (\text{B7})$$

with inverse transformation

$$\zeta_n = \frac{1}{\sqrt{N}} \sum_{k=0}^{N-1} q^{-(k+1/2)^2} q^{-2kn} \chi_k. \quad (\text{B8})$$

From Eq. (B7) we can easily see that

$$\chi_N = q^{(N+1/2)^2 - (1/2)^2} \chi_0, \quad (\text{B9})$$

which in combination with the the periodicity condition, Eq. (B4), it leads to

$$e^{-iN(\theta-\theta')} = q^{(N+1/2)^2 - (1/2)^2}, \quad (\text{B10})$$

and thus

$$N(\theta - \theta') + \pi P(N+1) = 0 \pmod{2\pi}. \quad (\text{B11})$$

Also, the inverse transformation is consistent as long as P and N are co-primes. Hence, for even and odd N , we have

$$\theta'_e = \theta + \pi\alpha + \frac{2\pi m}{N}, \quad (\text{B12})$$

$$\theta'_o = \theta + \frac{2\pi m}{N}, \quad (\text{B13})$$

for an arbitrary integer $m \in \mathbb{Z}$. Inserting Eq. (B7) into Eq. (B6) gives

$$\begin{aligned} & \sum_{n=0}^{N-1} \left[q^{(k-1/2)^2} q^{2(k-1)n} e^{i\theta'} + q^{(k+1/2)^2} q^{2k(n+1)} \right. \\ & \left. + q^{(k+1/2)^2} q^{2k(n-1)} + q^{(k+3/2)^2} q^{2(k+1)n} e^{-i\theta'} \right] \zeta_n \\ & = \epsilon \sum_{n=0}^{N-1} q^{(k+1/2)^2} q^{2kn} \zeta_n. \end{aligned} \quad (\text{B14})$$

For the first term we take $n' = n - 1$, which yields

$$\begin{aligned} & \sum_{n'=-1}^{N-2} q^{k^2 - k + 1/4} q^{2kn' - 2n' - 2 + 2k} e^{i\theta'} \zeta_{n'+1} = \\ & = \sum_{n'=-1}^{N-2} q^{(k+1/2)^2} q^{2kn'} q^{-2(n'+1)} e^{i\theta'} \zeta_{n'+1} = \\ & = \sum_{n'=0}^{N-1} q^{(k+1/2)^2} q^{2kn'} q^{-2(n'+1)} e^{i\theta'} \zeta_{n'+1}. \end{aligned} \quad (\text{B15})$$

The last step works by taking the choice $\zeta_0 = \zeta_N$. The other three terms can be similarly shifted to yield

$$\left(1 + e^{-i\theta'} q^{2n}\right) \zeta_{n-1} + \left(1 + e^{i\theta'} q^{-2(n+1)}\right) \zeta_{n+1} = \epsilon \zeta_n. \quad (\text{B16})$$

Now, we further apply another transformation

$$\zeta_n = q^{n(n+1)/2} e^{-in\theta'/2} \phi_n, \quad (\text{B17})$$

which after some algebra results in the following equation:

$$\cos\left(\pi\alpha n - \frac{\theta'}{2}\right) \phi_{n-1} + \cos\left(\pi\alpha(n+1) - \frac{\theta'}{2}\right) \phi_{n+1} = \frac{\epsilon}{2} \phi_n, \quad (\text{B18})$$

or equivalently

$$\begin{aligned} & \sin\left(\pi\alpha n + \frac{\pi - \theta'}{2}\right) \phi_{n-1} \\ & + \sin\left(\pi\alpha(n+1) + \frac{\pi - \theta'}{2}\right) \phi_{n+1} = \frac{\epsilon}{2} \phi_n, \end{aligned} \quad (\text{B19})$$

which is the desired sine model.

The boundary conditions from Eq. (B17) are $\phi_N = \phi_0 q^{-N(N+1)/2} e^{iN\theta'/2}$ and $\phi_{-1} = \phi_{N-1} q^{N(N-1)/2} e^{-iN\theta'/2}$.

The transformation is particularly simple for $\theta' = \pi$ in this case ϕ_{-1} and ϕ_N are disconnected from the rest of the chain, meaning that the boundary condition can be chosen arbitrarily. Therefore, using Eqs. (B12) and (B13), the above condition is satisfied by

$$\theta = \frac{\pi}{N}(N - P - 2m) \quad \text{for even } N, \quad (\text{B20})$$

$$\theta = \frac{\pi}{N}(N - 2m) \quad \text{for odd } N. \quad (\text{B21})$$

Since P and N cannot be both even (they are co-primes), both results above simplify to

$$\theta = (2m' + 1) \frac{\pi}{N}, \quad (\text{B22})$$

with $m' \in \mathbb{Z}$.

To summarize, the requirements for the transformations used in this case to work, are:

1. P and N are co-primes.
2. $\theta = (2m' + 1) \frac{\pi}{N}$ with $m' \in \mathbb{Z}$

These lead to the sine model used in the main paper

$$2 \sin(\pi\alpha n) \phi_{n-1} + 2 \sin(\pi\alpha(n+1)) \phi_{n+1} = \epsilon \phi_n. \quad (\text{B23})$$

Appendix C: Calculating the distribution of post-quench modes

In this section, we present the details of obtaining the distribution (expectation values of occupancy) of the post-quench modes. Let us denote the set of all single-particle eigenstates of the pre-quench Hamiltonian as $\{|\phi_\omega^{\text{pre}}\rangle\}$, which spans the full Hilbert space of size N , equal to the number of lattice points. The post-quench Hamiltonian, however, results in multiple causally-disconnected regions, with no Hamiltonian coupling terms between different regions.

After the quench, the full Hilbert space of N lattice points can be considered decomposed as $\mathcal{H}_0 = \bigoplus_{j=1}^m \mathcal{H}_j$, where each subspace corresponds to a different post-quench sub-region j . For each sub-region, we have separate sets of eigenstates $\{|\psi_E^{\text{post},j}\rangle\}$. Note that we assume the indices ω and E uniquely identify different eigenstates in both cases. In the context of a 1D sine model, we do not expect extensive degeneracies. However, in the event of degeneracies, we implicitly assume that ω and E are accompanied by an additional quantum number, allowing us to label all eigenstates accordingly.

Since both $\{|\phi_\omega^{\text{pre}}\rangle\}$ and $\bigoplus_j \{|\psi_E^{\text{post},j}\rangle\}$ span the full Hilbert space \mathcal{H}_0 , there exists a unitary transformation U that connects these sets of eigenstates:

$$|\psi_E^{\text{post},j}\rangle = \sum_{\omega} U_{(E,j);\omega} |\phi_\omega^{\text{pre}}\rangle, \quad (\text{C1})$$

$$|\phi_\omega^{\text{pre}}\rangle = \sum_{E,j} U_{\omega;(E,j)}^* |\psi_E^{\text{post},j}\rangle. \quad (\text{C2})$$

As mentioned earlier, the index ω and the double index (E, j) each take N different values.

Next, we demonstrate how to calculate the expectation values $\langle b_{E,j}^\dagger b_{E',j} \rangle \equiv \langle GS | b_{E,j}^\dagger b_{E',j} | GS \rangle$ for the post-quench modes. These operators, $b_{E,j}^\dagger$ and $b_{E',j}$, correspond to different eigenstates in subregion j , with respect to the ground state of the pre-quench Hamiltonian:

$$|GS\rangle = \prod_{\omega < 0} c_\omega^\dagger |0\rangle. \quad (\text{C3})$$

Here, c_ω^\dagger is the creation operator for a pre-quench energy eigenstate. Using Eq. (C1), we can immediately express the transformation between post- and pre-quench operators as:

$$\begin{aligned} b_{E,j}^\dagger &= \sum_{\omega} U_{(E,j);\omega} c_\omega^\dagger, \\ b_{E',j} &= \sum_{\omega} U_{(E',j);\omega}^* c_\omega. \end{aligned} \quad (\text{C4})$$

Substituting these expressions into the expectation values of the post-quench mode correlations, we obtain:

$$\begin{aligned} \langle b_{E,j}^\dagger b_{E',j} \rangle &= \sum_{\omega, \omega'} U_{(E,j);\omega} U_{(E',j);\omega'}^* \langle GS | c_\omega^\dagger c_{\omega'} | GS \rangle \\ &= \sum_{\omega < 0} U_{(E,j);\omega} U_{(E',j);\omega}^* \end{aligned} \quad (\text{C5})$$

This forms the basis for our numerical evaluation of the correlations and expectation values of mode occupations presented in the paper.

1. Even-odd effect dependence on sub-region size

We finally compare the results for a quench from a uniform hopping model ($P = 0$) to a sine hopping model ($P = 1$), when considering either even or odd numbers of lattice points inside each post-quench sub-region. Because the initial region in this quench scenario is twice as large as the initial one, the even and odd cases correspond to the initial lattice sizes being multiples of four and two (but not four), respectively. The main difference between these two cases is that with an odd number of sites and particle-hole symmetry, there exists a zero-energy mode, whereas in the even case, there is no zero-energy mode and instead we have a pair of states with small energies $\pm E_1$. Consequently, in the even case, the exact thermal form is not achieved for any finite lengths of the chain, as shown in Fig. 6.

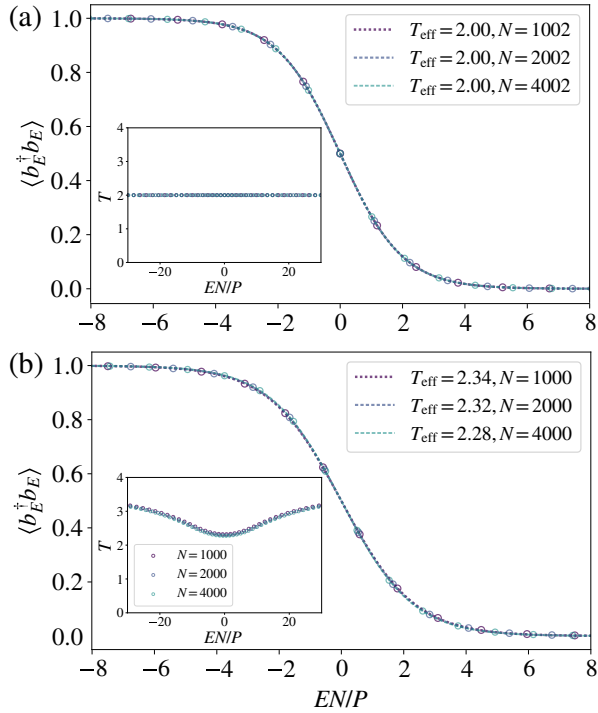


FIG. 6. Illustration of the even-odd dependence on the size of post-quench sub-regions. Panels (a) and (b) show the average occupation number and their thermal fit when we quench from the uniform hopping model ($P = 0$) to the sine model ($P = 1$), but with sizes such that the corresponding subregion size ($N/2$ in this case) is odd for panel (a) and even for panel (b).

It can be inferred from the trend of fitted effective temperatures for different N in Fig. 6(b), that increasing N leads to a slight decrease in the variation of effective temperatures. Hence, for very large N we expect the even-odd effect to disappear and the results for the two types of lattice sizes to reconcile. This type of even-odd effect, where the results slightly differ between cases where the size of the post-quench subregion of interest is even or odd, is a generic behavior of these models. We also found it to be present when we quench between two different values of the magnetic flux corresponding to two different values of P .

-
- [1] S. Sachdev and J. Ye, Gapless spin-fluid ground state in a random quantum heisenberg magnet, *Phys. Rev. Lett.* **70**, 3339 (1993).
- [2] A. Kitaev, A simple model of quantum holography, in *KITP strings seminar and Entanglement*, Vol. 12 (2015) p. 26.
- [3] A. Kitaev and S. J. Suh, The soft mode in the sachdev-ye-kitaev model and its gravity dual, *J. High Energy Phys.* **2018** (5), 183.
- [4] J. Maldacena and D. Stanford, Remarks on the sachdev-ye-kitaev model, *Phys. Rev. D* **94**, 106002 (2016).
- [5] J. Maldacena, D. Stanford, and Z. Yang, Conformal symmetry and its breaking in two-dimensional nearly anti de sitter space, *Prog. Theo. Exp. Phys.* **2016**, 12C104 (2016).
- [6] N. P. Armitage, E. J. Mele, and A. Vishwanath, Weyl and dirac semimetals in three-dimensional solids, *Rev. Mod. Phys.* **90**, 015001 (2018).
- [7] G. E. Volovik, Black hole and hawking radiation by type-ii weyl fermions, *JETP Lett.* **104**, 645 (2016).
- [8] G. E. Volovik, *The universe in a helium droplet*, Vol. 117 (Oxford University Press, Oxford, 2003).
- [9] A. Westström and T. Ojanen, Designer curved-space geometry for relativistic fermions in weyl metamaterials, *Phys. Rev. X* **7**, 041026 (2017).
- [10] S. A. Hartnoll, Horizons, holography and condensed matter (2011), [arXiv:1106.4324](https://arxiv.org/abs/1106.4324) [hep-th].
- [11] S. Guan, Z.-M. Yu, Y. Liu, G.-B. Liu, L. Dong, Y. Lu, Y. Yao, and S. A. Yang, Artificial gravity field, astrophysical analogues, and topological phase transitions in strained topological semimetals, *npj Quantum Mater.* **2**, 1 (2017).
- [12] H. Huang, K.-H. Jin, and F. Liu, Black-hole horizon in the dirac semimetal $\text{Zn}_2\text{In}_2\text{S}_5$, *Phys. Rev. B* **98**, 121110 (2018).
- [13] L. Liang and T. Ojanen, Curved spacetime theory of inhomogeneous weyl materials, *Phys. Rev. Research* **1**, 032006 (2019).
- [14] A. Haller, S. Hegde, C. Xu, C. D. Beule, T. L. Schmidt, and T. Meng, Black hole mirages: Electron lensing and Berry curvature effects in inhomogeneously tilted Weyl semimetals, *SciPost Phys.* **14**, 119 (2023).
- [15] V. Könye, L. Mertens, C. Morice, D. Chernyavsky, A. G. Moghaddam, J. van Wezel, and J. van den Brink, Anisotropic optics and gravitational lensing of tilted weyl fermions, *Phys. Rev. B* **107**, L201406 (2023).
- [16] V. Könye, C. Morice, D. Chernyavsky, A. G. Moghaddam, J. van den Brink, and J. van Wezel, Horizon physics of quasi-one-dimensional tilted weyl cones on a lattice, *Phys. Rev. Res.* **4**, 033237 (2022).
- [17] Y. Kedem, E. J. Bergholtz, and F. Wilczek, Black and white holes at material junctions, *Phys. Rev. Research* **2**, 043285 (2020).
- [18] C. Morice, A. G. Moghaddam, D. Chernyavsky, J. van

- Wezel, and J. van den Brink, Synthetic gravitational horizons in low-dimensional quantum matter, *Phys. Rev. Research* **3**, L022022 (2021).
- [19] C. Morice, D. Chernyavsky, J. van Wezel, J. van den Brink, and A. G. Moghaddam, Quantum dynamics in 1D lattice models with synthetic horizons, *SciPost Phys. Core* **5**, 042 (2022).
- [20] J. Hu, L. Feng, Z. Zhang, and C. Chin, Quantum simulation of unruh radiation, *Nat. Phys.* **15**, 785 (2019).
- [21] J. Steinhauer, Observation of quantum hawking radiation and its entanglement in an analogue black hole, *Nat. Phys.* **12**, 959 (2016).
- [22] J. Nissinen, Emergent spacetime and gravitational nihyan anomaly in chiral $p + ip$ weyl superfluids and superconductors, *Phys. Rev. Lett.* **124**, 117002 (2020).
- [23] C. Barceló, S. Liberati, and M. Visser, Analogue gravity from bose-einstein condensates, *Class. Quantum Gravity* **18**, 1137 (2001).
- [24] C. Barceló, S. Liberati, and M. Visser, Analogue gravity, *Living Rev. Relativ.* **14**, 3 (2011).
- [25] I. Carusotto, S. Fagnocchi, A. Recati, R. Balbinot, and A. Fabbri, Numerical observation of hawking radiation from acoustic black holes in atomic bose-einstein condensates, *New J. Phys.* **10**, 103001 (2008).
- [26] H. S. Nguyen, D. Gerace, I. Carusotto, D. Sanvitto, E. Galopin, A. Lemaître, I. Sagnes, J. Bloch, and A. Amo, Acoustic black hole in a stationary hydrodynamic flow of microcavity polaritons, *Phys. Rev. Lett.* **114**, 036402 (2015).
- [27] J. Dubail, J.-M. Stéphan, and P. Calabrese, Emergence of curved light-cones in a class of inhomogeneous Luttinger liquids, *SciPost Phys.* **3**, 019 (2017).
- [28] J. Minář and B. Grémaud, Mimicking dirac fields in curved spacetime with fermions in lattices with non-unitary tunneling amplitudes, *Journal of Physics A: Mathematical and Theoretical* **48**, 165001 (2015).
- [29] T. Farajollahpour, Z. Faraei, and S. A. Jafari, Solid-state platform for space-time engineering: The $8pmmn$ borophene sheet, *Phys. Rev. B* **99**, 235150 (2019).
- [30] M. Stålhammar, J. Larana-Aragon, L. Rødland, and F. K. Kunst, PT symmetry-protected exceptional cones and analogue Hawking radiation, *New J. Phys.* **25**, 043012 (2023).
- [31] M. D. Horner, A. Hallam, and J. K. Pachos, Chiral spin-chain interfaces exhibiting event-horizon physics, *Phys. Rev. Lett.* **130**, 016701 (2023).
- [32] A. Daniel, A. Hallam, M. D. Horner, and J. K. Pachos, Optimally scrambling chiral spin-chain with effective black hole geometry, *Scientific Reports* **15**, 9103 (2025).
- [33] T. G. Philbin, C. Kuklewicz, S. Robertson, S. Hill, F. König, and U. Leonhardt, Fiber-optical analog of the event horizon, *Science* **319**, 1367 (2008).
- [34] A. Roldán-Molina, A. S. Nunez, and R. A. Duine, Magnonic black holes, *Phys. Rev. Lett.* **118**, 061301 (2017).
- [35] A. J. Kollár, M. Fitzpatrick, and A. A. Houck, Hyperbolic lattices in circuit quantum electrodynamics, *Nature* **571**, 45 (2019).
- [36] I. Boettcher, P. Bienias, R. Belyansky, A. J. Kollár, and A. V. Gorshkov, Quantum simulation of hyperbolic space with circuit quantum electrodynamics: From graphs to geometry, *Phys. Rev. A* **102**, 032208 (2020).
- [37] I. Boettcher, A. V. Gorshkov, A. J. Kollár, J. Maciejko, S. Rayan, and R. Thomale, Crystallography of hyperbolic lattices, *Phys. Rev. B* **105**, 125118 (2022).
- [38] L. Mertens, A. G. Moghaddam, D. Chernyavsky, C. Morice, J. van den Brink, and J. van Wezel, Thermalization by a synthetic horizon, *Phys. Rev. Res.* **4**, 043084 (2022).
- [39] P. B. Wiegmann and A. V. Zabrodin, Bethe-ansatz for the bloch electron in magnetic field, *Phys. Rev. Lett.* **72**, 1890 (1994).
- [40] I. V. Krasovskiy, Bethe ansatz for the Harper equation: Solution for a small commensurability parameter, *Phys. Rev. B* **59**, 322 (1999).
- [41] X. Wen and A. Zee, Winding number, family index theorem, and electron hopping in a magnetic field, *Nuclear Physics B* **316**, 641 (1989).
- [42] Y. Hatsugai and M. Kohmoto, Energy spectrum and the quantum hall effect on the square lattice with next-nearest-neighbor hopping, *Phys. Rev. B* **42**, 8282 (1990).
- [43] P. G. Harper, Single band motion of conduction electrons in a uniform magnetic field, *Proceedings of the Physical Society. Section A* **68**, 874 (1955).
- [44] D. R. Hofstadter, Energy levels and wave functions of bloch electrons in rational and irrational magnetic fields, *Physical review B* **14**, 2239 (1976).
- [45] D. Tong, Lectures on the quantum hall effect, arXiv:1606.06687 (2016).
- [46] V. Könye, L. Mertens, C. Morice, D. Chernyavsky, A. G. Moghaddam, J. van Wezel, and J. van den Brink, Anisotropic optics and gravitational lensing of tilted weyl fermions, *Phys. Rev. B* **107**, L201406 (2023).
- [47] V. Könye, C. Morice, D. Chernyavsky, A. G. Moghaddam, J. van den Brink, and J. van Wezel, Horizon physics of quasi-one-dimensional tilted weyl cones on a lattice, *Phys. Rev. Res.* **4**, 033237 (2022).
- [48] S. W. Hawking, Black hole explosions?, *Nature* **248**, 30 (1974).
- [49] W. G. Unruh, Notes on black-hole evaporation, *Phys. Rev. D* **14**, 870 (1976).
- [50] W. Israel, Thermo-field dynamics of black holes, *Phys. Lett. A* **57**, 107 (1976).
- [51] L. Bombelli, R. K. Koul, J. Lee, and R. D. Sorkin, Quantum source of entropy for black holes, *Phys. Rev. D* **34**, 373 (1986).
- [52] S. Takagi, Vacuum Noise and Stress Induced by Uniform Acceleration: Hawking-Unruh Effect in Rindler Manifold of Arbitrary Dimension, *Progress of Theoretical Physics Supplement* **88**, 1 (1986).
- [53] V. P. Frolov and D. V. Fursaev, Thermal fields, entropy and black holes, *Class. Quantum Gravity* **15**, 2041 (1998).
- [54] R. B. Mann, *Black holes: thermodynamics, information, and firewalls* (Springer, 2015).
- [55] G. Wong, I. Klich, L. A. P. Zayas, and D. Vaman, Entanglement temperature and entanglement entropy of excited states, *Journal of High Energy Physics* **2013**, 20 (2013).
- [56] J. Cardy and E. Tonni, Entanglement hamiltonians in two-dimensional conformal field theory, *J. Stat. Mech.: Theory Exp.* **2016** (12), 123103.
- [57] V. Eisler and I. Peschel, Properties of the entanglement hamiltonian for finite free-fermion chains*, *J. Stat. Mech.: Theory Exp.* **2018** (10), 104001.
- [58] V. Eisler, E. Tonni, and I. Peschel, On the continuum limit of the entanglement hamiltonian, *J. Stat. Mech.:*

[Theory Exp. 2019 \(7\), 073101.](#)

- [59] J. J. Bisognano and E. H. Wichmann, On the duality condition for a hermitian scalar field, *Journal of Mathematical Physics* **16**, 985 (1975).
- [60] M. Dalmonte, V. Eisler, M. Falconi, and B. Vermersch, Entanglement hamiltonians: From field theory to lattice models and experiments, *Ann. Phys. (Berl.)* **534**, 2200064 (2022).
- [61] A. G. Moghaddam, K. Pöyhönen, and T. Ojanen, Boiling quantum vacuum: Thermal subsystems from ground-state entanglement, *PRX Quantum* **3**, 030335 (2022).
- [62] We use absolute fitting error $\chi^2 = \sum_i [f_i - f_{\text{FD}}(E_i, T_{\text{eff}})]^2$ with f_i denoting the numerically calculated post-quench occupation and f_{FD} the Fermi-Dirac function with a fitted temperature T_{eff} .
- [63] M. Aidelsburger, M. Atala, M. Lohse, J. T. Barreiro, B. Paredes, and I. Bloch, Realization of the Hofstadter Hamiltonian with Ultracold Atoms in Optical Lattices, *Phys. Rev. Lett.* **111**, 185301 (2013).
- [64] M. Aidelsburger, M. Lohse, C. Schweizer, M. Atala, J. T. Barreiro, S. Nascimbène, N. Cooper, I. Bloch, and N. Goldman, Measuring the Chern number of Hofstadter bands with ultracold bosonic atoms, *Nat. Phys.* **11**, 162 (2015).
- [65] It should be noted that this Hamiltonian is manifestly Hermitian as the second term $\sin(\pi(\hat{x} + 1)\alpha)e^{i\hat{p}}$ can be also re-written as $e^{i\hat{p}}\sin(\pi\hat{x}\alpha)$ which is the Hermitian conjugate of the first term.